Coherent backscattering of light from a Faraday medium

E. E. Gorodnichev and K. A. Kondratiev
Department of Theoretical Physics, National Research Nuclear University MEPhI, Kashirskoe Shosse 31, 115409 Moscow, Russia

D. B. Rogozkin
Department of Theoretical Physics, National Research Nuclear University MEPhI, Kashirskoe Shosse 31, 115409 Moscow, Russia
and Dukhov Research Institute of Automatics (VNIIA), Sushchevskaya ulitza 22, 127055 Moscow, Russia

(Received 2 November 2021; revised 21 February 2022; accepted 15 March 2022; published 30 March 2022)

We study coherent backscattering (CBS) of light from a magnetoactive medium doped by Mie particles. A novel version of the CBS diffusion theory is developed, which takes into account both the Faraday effect and the effect of circular polarization memory specific to Mie scattering. The theory is based on a system of coupled diffusion equations for two slowly decaying cooperon modes arising from interference of waves with coinciding helicities. The impact of a magnetic field on CBS is shown to be controlled by the ratio of the helicity-flip scattering cross section to the transport scattering one. If this ratio is small, the CBS can exhibit unusual features first found experimentally by R. Lenke, R. Lehner, and G. Maret [Europhys. Lett. **52**, 620 (2000)]. In the magnetic field parallel to the sample surface, the peak of coherent backscattering for circularly polarized light is shifted from the exact backward direction, while, for linearly polarized light, it splits in two ones for both co- and cross-polarization channels, and the backscattered waves acquire circular polarization. Saturation of the magnetic field dependence of the CBS cone occurs in the magnetic field normal to the surface. If the above ratio is close to unity (Rayleigh scattering) all these features disappear, and the effect of the magnetic field on the CBS angular profile is reduced to the universal law studied previously. The results obtained are in good quantitative agreement with the available Monte Carlo simulation and experimental data.

DOI: 10.1103/PhysRevB.105.104208

I. INTRODUCTION

Magnetic field effects play a key role in mesoscopic physics [1–4]. A magnetic field violates the time-reversal symmetry and enables controlling the interference of waves propagating in disordered structures. This reveals itself in electron transport through solids where the Aharonov-Bohm effect underlies the mechanism for manipulating the interference of electronic waves [1–3,5,6], as well as in propagation of electromagnetic waves in magnetoactive materials [4,7–13].

In multiple scattering of light by disordered media, the constructive interference of time-reversed waves causes the effect of coherent enhancement of backscattering [3,4,14–16]. In magnetoactive media, due to the Faraday effect, waves with different helicity acquire phase shifts of the opposite sign, which leads to suppression of wave interference and, as a result, smoothing of the peak in the CBS angular profile. The magnetic field effect on CBS was studied in detail theoretically for Rayleigh scatterers embedded in a magnetoactive medium [17–20] and was also observed in experiments [21,22]. Another example of a system where the Faraday effect affects wave propagation is a disordered medium composed of magnetoactive particles [23–26].

Among the studies of the magnetic field effect on CBS, experiment [27] on light scattering by Mie spheres in magnetoactive glass should be highlighted where a displacement and splitting of the CBS peak were observed depending on the polarization state of the incident light. Although a key role of circular polarization memory has been noted in Ref. [27] (see also Ref. [22]), no theoretical explanation for the experimental data of Ref. [27] has yet been given.

It is commonly accepted that the magnetic field destroys the CBS effect [4,17–26]. This conclusion was drawn for the case of Rayleigh scattering, in which a change in the helicity of light occurs virtually in every scattering event [4,17–19]. However, if depolarization is turned off (for example, under conditions of the circular polarization memory effect, see, e.g., Refs. [28–32]), the magnetic field does not destroy the interference of waves with a given helicity, but only leads to the appearance of an additional phase shift between two time-reversed waves.

In a magnetic field, the Green's function that describes wave propagation between two scattering events can be written as (see, e.g., Refs. [18,19])

$$\langle G_{ik}(\mathbf{r})\rangle = \langle G_{\rm scal}(\mathbf{r})\rangle [P_{ik}^{(+)}(\mathbf{n}) e^{-\frac{i}{2}\,\mathbf{hr}} + P_{ik}^{(-)}(\mathbf{n}) e^{\frac{i}{2}\,\mathbf{hr}}], \quad (1)$$

where $\langle G_{\rm scal}(\mathbf{r})\rangle$ is the Green's function for scalar waves [3,15,16], the brackets $\langle \ldots \rangle$ denote averaging over random positions of scattering centers, $\mathbf{n} = \mathbf{r}/|\mathbf{r}|$, and

$$P_{ik}^{(\pm)}(\mathbf{n}) = \tfrac{1}{2}(\delta_{ik} - n_i n_k \pm i e_{ikj} n_j) \quad (2)$$

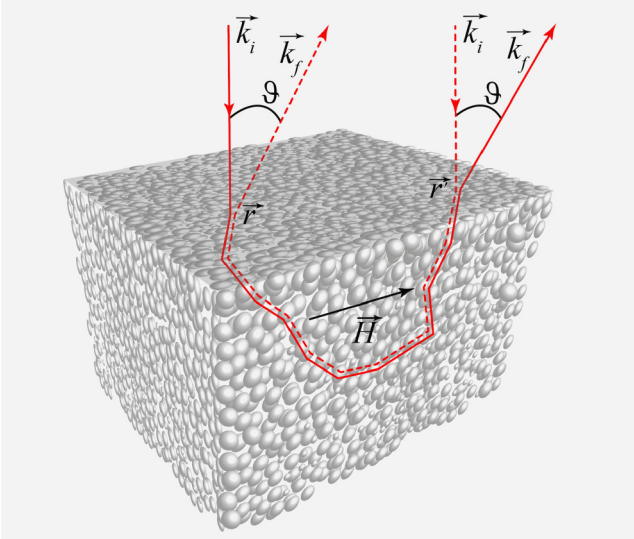

FIG. 1. Geometry of coherent backscattering. The wave field and its time-reversed counterpart are shown with solid and dashed lines, respectively. Magnetic field **H** is parallel to the surface.

are the projection operators on the states of light with a given helicity (i.e., on the right-handed and left-handed circularly polarized components of the field), e_{ikj} is the antisymmetric Levi-Civita tensor. The far-field condition, $k_0 r \gg 1$ (k_0 is the wave number), is implied in Eq. (1). The vector **h** appearing in Eq. (1) is equal to $\mathbf{h} = 2V\mathbf{H}$, where V is the Verdet constant (see, e.g., Refs. [33,34]) and **H** is the magnetic field strength. According to Eq. (1), if the helicity of waves remains unchanged in multiple scattering, the constructive interference of the waves with the same helicity occurs independently.

In coherent backscattering from a magnetoactive medium, the shift between the phases of two time-reversed waves with a given helicity (see Fig. 1) has the form

$$\Delta\varphi(\mathbf{r}, \mathbf{r}') = \mathbf{q} \cdot (\mathbf{r} - \mathbf{r}') \pm \mathbf{h} \cdot (\mathbf{r} - \mathbf{r}'), \tag{3}$$

where **q** is the projection of the wave vector $\mathbf{k}_f$ of the backscattered light onto the medium surface, and the magnetic field is assumed to be uniform. The first term appearing in the right-hand side of Eq. (3) is the same phase shift as in the scalar case [3] (see, also, Refs. [14–16]). The second term is due to the Faraday effect. The sign before the second term is determined by the circular polarization of the incident wave, clockwise or counterclockwise (i.e., by the helicity).

The interference contribution to the backscattering intensity is obtained by summing over all time-reversed wave paths (see, e.g., Refs. [3,14]). While retaining helicity, in accordance with Eq. (3), the magnetic field effect on the interference contribution is reduced to the argument shift,

$$J_{\pm}^{(c)} = J_{\mathrm{scal}}^{(c)}(\mathbf{q} \pm \mathbf{h}_{\parallel}), \tag{4}$$

where $J_{\mathrm{scal}}^{(c)}(\mathbf{q})$ is the interference contribution to the backscattering intensity calculated in the scalar approximation with no magnetic field [3,4,14–16], $\mathbf{h}_{\parallel}$ is the projection of the vector **h** onto the sample surface. As follows from Eq. (4), the magnetic field does not lead to suppression of interference, but results in a displacement of the coherent backscattering peak by the angle $\Delta\vartheta = \pm h/k_0$ from the backward direction. A similar effect was found in CBS of electrons [35] where the peak displacement is due to a nonzero average magnetic flux through the loop formed by time-reversed electron trajectories and is a consequence of the Aharonov-Bohm effect.

For linearly polarized light, which can be represented as superposition of two fields with opposite circular polarizations, the CBS intensity is determined by the relation

$$J_L^{(c)} = \tfrac{1}{2}\big(J_{\mathrm{scal}}^{(c)}(\mathbf{q} + \mathbf{h}_{\parallel}) + J_{\mathrm{scal}}^{(c)}(\mathbf{q} - \mathbf{h}_{\parallel})\big). \tag{5}$$

According to Eq. (5), two peaks at $\vartheta_{\mathrm{peak}} = \pm h/k_0$ appear in the angular profile of the intensity. The fact that the displacement and splitting of the CBS cone [see Eqs. (4) and (5), respectively] occurs due to waves with retaining helicity was first pointed out in Refs. [22,27].

Depolarization changes the simple results (4) and (5), but the constructive interference is not completely destroyed. In this paper we develop a two-mode diffusion theory of wave interference in a multiply scattering magnetoactive medium. Each mode corresponds to the interference contribution (cooperon) of time-reversed waves with a given helicity to the density matrix of backscattered light and obeys a system of coupled diffusion equations. An analytical solution to these equations is obtained for different orientations of the magnetic field relative to the sample surface. The magnetic field effect on CBS is shown to be controlled by the ratio of the helicity-flip scattering cross section to the transport scattering one. If this ratio is small, the CBS exhibits specific features similar to those that follow from Eqs. (4) and (5). In the magnetic field parallel to the sample surface, the CBS peak for circularly polarized light is shifted from the exact backward direction, while, for linearly polarized light, it splits into two ones, wherein the backscattered waves acquire circular polarization. In the field normal to the sample surface, the magnetic field dependence of the CBS cone is saturated. The difference between the CBS angular profiles for linearly co- and cross-polarized waves disappears as the field strength increases. If the helicity-flip scattering cross section and the transport scattering one are of the same order (e.g., for Rayleigh scattering) all these features vanish, and the effect of the magnetic field on the CBS angular profile is reduced to the universal law studied previously [17,19]. The results obtained are in good quantitative agreement with the available experimental and Monte Carlo simulation data [20,27].

II. THEORETICAL MODEL

Consider multiple scattering of a plane electromagnetic wave incident on a nonabsorbing magnetoactive medium along the inward normal $\mathbf{n}_0$ to the surface. The coherent contribution to the intensity of backscattered waves is governed by the sum of the most-crossed diagrams $\langle G_{ik}(\mathbf{r}, \mathbf{r}'|\mathbf{h}) G_{jl}^*(\mathbf{r}_1, \mathbf{r}_1'|\mathbf{h})\rangle_C$ (see, e.g., Refs. [3,16–19]), which can be expressed in terms of the sum of ladder diagrams (see Fig. 2) by rearranging coordinates and indices and changing the sign of the magnetic field [17,18],

$$\langle G_{ik}(\mathbf{r}, \mathbf{r}'|\mathbf{h}) G_{jl}^*(\mathbf{r}_1, \mathbf{r}_1'|\mathbf{h})\rangle_C = \langle G_{ik}(\mathbf{r}, \mathbf{r}'|\mathbf{h}) G_{lj}^*(\mathbf{r}_1', \mathbf{r}_1|-\mathbf{h})\rangle_L, \tag{6}$$

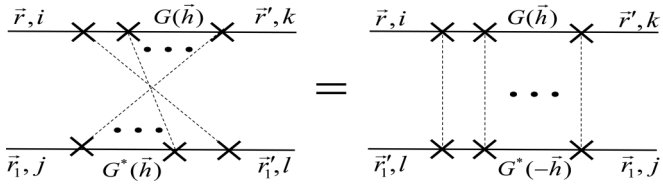

FIG. 2. Relation between most-crossed and ladder diagrams.

where the brackets $\langle \ldots \rangle$ denote averaging over random positions of scattering centers. The sum of ladder diagrams $\Gamma^{(c)} = \langle G(\mathbf{h})G^*(-\mathbf{h})\rangle_L$ is subject to the integral equation (see Fig. 11 and Appendix A).

The intensity and the polarization state of light in the CBS cone are determined by the density matrix [19,36,37]

$$J_{ij}^{(c)}(\mathbf{q}) = \Gamma_{il,kj}^{(c)}(\mathbf{q}|-\mathbf{n}_0,\mathbf{n}_0)|_\Sigma \rho_{kl}^{(0)}, \tag{7}$$

where summation over repeated indices is implied, $\Gamma^{(c)}|_\Sigma = \Gamma_{il,kj}^{(c)}(z=0,z'=0,\mathbf{q}|-\mathbf{n}_0,\mathbf{n}_0)$ is the value of the ladder propagator at the surface of the medium in the exact backward direction [38], $\rho_{kl}^{(0)}$ is the density matrix of the incident electromagnetic field.

When calculating the propagator $\Gamma^{(c)}$ we take advantage of two approximations. We suppose that the condition of circular polarization memory [28–32] is fulfilled (i.e., the helicity-flip scattering cross section $\sigma_{\rm dep}$ [30] is much less then the transport scattering cross-section σ_{tr}). Under this condition, two modes corresponding to the interference of waves with the same helicity, decay over path lengths much longer than the transport mean-free path and make the main contribution to the intensity of backscattered light [39]. In our calculations, we take into account only these two long-lived modes [40]. Within the two-mode approximation the propagator $\Gamma^{(c)}$ appearing in Eq. (7) can be represented in the form [see Appendix A, Eqs. (A5) and (A6)]

$$\Gamma_{il,kj}^{(c)}(z,z',\mathbf{q}|-\mathbf{n}_0,\mathbf{n}_0) = \sum_{\alpha,\beta=+,-} P_{il}^{(\alpha)}(-\mathbf{n}_0)\Gamma_{\alpha\beta}^{(c)}(z,z',\mathbf{q}|-\mathbf{n}_0,\mathbf{n}_0)P_{jk}^{(\beta)}(\mathbf{n}_0), \tag{8}$$

where the summation is performed over modes with a given helicity, the projection operators $P_{ik}^{(\pm)}(\mathbf{n})$ are defined by Eq. (2), the propagator $\Gamma_{\alpha\beta}^{(c)}$ describes the interference of waves with coinciding helicities. Then the density matrix (7) of backscattered waves takes the form

$$J_{ij}^{(c)}(\mathbf{q}) = \sum_{\alpha,\beta} J_{\alpha\beta}^{(c)}(\mathbf{q})\rho_{ij}^{(\alpha\beta)}, \tag{9}$$

where

$$J_{\alpha\beta}^{(c)}(\mathbf{q}) = \Gamma_{\alpha\beta}^{(c)}(z=0,z'=0,\mathbf{q}|-\mathbf{n}_0,\mathbf{n}_0)$$

and

$$\rho_{ij}^{(\alpha\beta)} = P_{il}^{(\alpha)}(-\mathbf{n}_0)\rho_{kl}^{(0)}P_{jk}^{(\beta)}(\mathbf{n}_0). \tag{10}$$

The density matrix $\rho_{ij}^{(\alpha\beta)}$ can be expressed in terms of circular components $E_\pm^{(0)}$ of the electric field [see also Appendix A, Eq. (A4)] in the incident wave,

$$\rho_{ij}^{(\pm\pm)} = \frac{1}{2}|E_\pm^{(0)}|^2\begin{pmatrix}1 & \mp i\\ \pm i & 1\end{pmatrix}, \tag{11}$$

$$\rho_{ij}^{(+-)} = (\rho_{ij}^{(c)-+})^* = \frac{1}{2}E_-^{(0)}(E_+^{(0)})^*\begin{pmatrix}1 & i\\ i & -1\end{pmatrix}. \tag{12}$$

Equations (11) and (12) refers to the Cartesian coordinate system with the z axis directed along the inward normal to the sample surface.

As the modes with a given helicity decay over path lengths exceeding the transport mean-free path we can apply the diffusion approximation to their calculations. Based on the standard procedure for calculating the backscattering intensity within the diffusion theory (see, e.g., Refs. [3,14–16,19,39]) we represent $J_{\alpha\beta}^{(c)}(\mathbf{q})$ in the form

$$J_{\alpha\beta}^{(c)}(\mathbf{q}) = \frac{1}{4\pi}\int_0^L \frac{dz}{l_{tr}}\int_0^L \frac{dz'}{l_{tr}} \times \exp\left[-\frac{z+z'}{l_{tr}} - ih_z(\beta z - \alpha z')\right]\Gamma_{\alpha\beta}^{(c)}(z,z'|\mathbf{q}), \tag{13}$$

where $\Gamma_{\alpha\beta}^{(c)}(z,z'|\mathbf{q})$ is a density propagator (integral over angles) for modes with a given helicity, $\Gamma_{\alpha\beta}^{(c)}(z,z'|\mathbf{q})$ obeys two coupled diffusion equations (see Appendix A)

$$\begin{pmatrix}\left(i\frac{\partial}{\partial z}+h_z\right)^2 + (\mathbf{q}-\mathbf{h}_\parallel)^2 + 3/(2l_{tr}l_{\rm dep}) & -3/(2l_{tr}l_{\rm dep})\\ -3/(2l_{tr}l_{\rm dep}) & \left(i\frac{\partial}{\partial z}-h_z\right)^2 + (\mathbf{q}+\mathbf{h}_\parallel)^2 + 3/(2l_{tr}l_{\rm dep})\end{pmatrix}\begin{pmatrix}\Gamma_{++}(z,z'|\mathbf{q}) & \Gamma_{+-}(z,z'|\mathbf{q})\\ \Gamma_{-+}(z,z'|\mathbf{q}) & \Gamma_{--}(z,z'|\mathbf{q})\end{pmatrix} = \frac{3}{l_{tr}}\begin{pmatrix}1 & 0\\ 0 & 1\end{pmatrix}\delta(z-z'), \tag{14}$$

where $h_z = (\mathbf{h}\mathbf{n}_0)$, $l_{tr} = (n_0\sigma_{tr})^{-1}$ is the transport mean-free path, $l_{\rm dep} = (n_0\sigma_{\rm dep})^{-1}$ is the mean-free path with respect to helicity-flip scattering, n_0 is the number of particles per unit volume. Formulas for calculating the cross sections σ_{tr} and $\sigma_{\rm dep}$ are given in Appendix A [see Eqs. (A14) and (A15)]. It is assumed that the sample thickness L is much greater than the transport mean-free path l_{tr}, $L \gg l_{tr}$. Equation (13) satisfies the condition $J_{\alpha\beta}^{(c)}(\mathbf{q},\mathbf{h}) = J_{-\alpha-\beta}^{(c)}(\mathbf{q},-\mathbf{h})$, which is a consequence of time-reversal symmetry [3,43,44].

By definition, the elements of the density matrix $J_{ij}^{(c)}(\mathbf{q})$ are directly related to the coherent contributions $I^{(c)}$, $Q^{(c)}$, $U^{(c)}$, and $V^{(c)}$ into the Stokes parameters in the CBS cone (see, e.g.,

Ref. [41]),

$$J_{ij}^{(c)}(\mathbf{q}) = \frac{1}{2}\begin{pmatrix} I^{(c)}(\mathbf{q}) + Q^{(c)}(\mathbf{q}) & U^{(c)}(\mathbf{q}) + iV^{(c)}(\mathbf{q}) \\ U^{(c)}(\mathbf{q}) - iV^{(c)}(\mathbf{q}) & I^{(c)}(\mathbf{q}) - Q^{(c)}(\mathbf{q}) \end{pmatrix}. \tag{15}$$

The multipliers before the matrices appearing in Eqs. (11) and (12) can also be expressed in terms of the Stokes parameters of the incident light, $|E_{\pm}^{(0)}|^2 = (I^{(0)} \mp V^{(0)})/2$ and $E_{-}^{(0)}(E_{+}^{(0)})^* = (Q^{(0)} - iU^{(0)})/2$.

For the incident circularly polarized light ($E_+ = 1$, $E_- = 0$, helicity is $+1$ if the light is polarized clockwise or $E_+ = 0$, $E_- = 1$, helicity is -1 if light is polarized counterclockwise [49]), matrices (12) are equal to zero. From Eqs. (9) and (11) it follows that the coherent backscattering occurs in this case only in the helicity-preserving channel. The intensity of backscattered light is determined by the elements $J_{\pm\pm}^{(c)}(\mathbf{q})$. In the considered approximation, the CBS intensity in the opposite helicity channel is neglected, which agrees with data of numerical calculations and experiments (see, e.g., Refs. [20,39,41] and references therein) for Mie scatterers.

For the incident linearly polarized beam, the values of E_+ and E_- appearing in Eqs. (11) and (12) are equal to each other, $E_+ = E_- = 1/\sqrt{2}$. The intensities of the co- and cross-polarized components of the backscattered waves are determined by the diagonal elements $J_{xx}^{(c)}(\mathbf{q})$ and $J_{yy}^{(c)}(\mathbf{q})$ of the matrix (9) [or (15)], respectively, and, according to Eq. (9), are equal to

$$J_{\parallel,\perp}^{(c)}(\mathbf{q}) = \tfrac{1}{4}(J_{++}^{(c)}(\mathbf{q}) \pm J_{-+}^{(c)}(\mathbf{q}) \pm J_{+-}^{(c)}(\mathbf{q}) + J_{--}^{(c)}(\mathbf{q})). \tag{16}$$

The intensity of backscattered waves with a given helicity is expressed in terms of the elements of the matrix (9) as

$$J_{\pm}^{(c)}(\mathbf{q}) = \tfrac{1}{2}\left[J_{xx}^{(c)}(\mathbf{q}) + J_{yy}^{(c)}(\mathbf{q}) \pm i\left(J_{xy}^{(c)}(\mathbf{q}) - J_{yx}^{(c)}(\mathbf{q})\right)\right] \tag{17}$$

or, with allowance for Eqs. (11) and (12), as

$$J_{\pm}^{(c)}(\mathbf{q}) = \tfrac{1}{2}\, J_{\pm\pm}^{(c)}(\mathbf{q}). \tag{18}$$

In the diffusion regime, a magnetic field does not affect the intensity and polarization state of incoherently scattered light [17,19]. In this case, the phase shifts resulting from the magnetic field in the Green's functions (1) are canceled out. In the backward direction, the density matrix is determined by the relation (see, also, Ref. [39])

$$J_{ij}^{(\mathrm{in})} = \sum_{\alpha,\beta} J_{\alpha\beta}^{(\mathrm{in})} \tilde{\rho}_{ij}^{(\alpha\beta)}, \tag{19}$$

where $J_{\alpha\beta}^{(\mathrm{in})} = J_{\alpha\beta}^{(c)}(\mathbf{q} = 0, \mathbf{h} = 0)$, and $\tilde{\rho}_{ij}^{(\alpha\beta)} = P_{ij}^{(\alpha)}(-\mathbf{n}_0)P_{kl}^{(\beta)}(\mathbf{n}_0)\rho_{kl}^{(0)}$, or $\tilde{\rho}_{ij}^{(\pm\pm)} = \rho_{ij}^{(\pm\pm)}$ and $\tilde{\rho}_{ij}^{(\mp\pm)} = (\rho_{ij}^{(\pm\pm)})^*$. Matrix elements $J_{\alpha\beta}^{(\mathrm{in})}$ were calculated in Ref. [39].

III. RESULTS

For an arbitrary orientation of the magnetic field, a solution of the diffusion equations for $\Gamma_{\alpha\beta}(z, z'|\mathbf{q})$ [see Eq. (14)] looks rather cumbersome. Therefore we present here analytical solutions of these equations and the corresponding CBS angular profiles for the two important cases (see, e.g., Refs. [20,27]) where the magnetic field is directed, respectively, parallel and perpendicular to the sample surface.

A. Angular profile of CBS in magnetic field parallel to the surface

In the magnetic field parallel to the sample surface, $h_z = 0$ (the Voigt geometry, see, e.g., Refs. [9,45]), Eq. (14) for $\Gamma_{\alpha\beta}(z, z'|\mathbf{q})$ can be reduced to a diagonal form (e.g., in the same way as it is done when going to normal coordinates in the theory of harmonic oscillations [46]). As a result, the matrix elements $\Gamma_{\alpha\beta}(z, z'|\mathbf{q})$ are expressed in terms of a linear combination of two functions $P_{\pm}(z, z'|\mathbf{q})$

$$\Gamma_{\pm\pm}(z, z'|\mathbf{q}) = \frac{\mathcal{M}_{\pm}}{\mathcal{N}} P_{+}(z, z'|\mathbf{q}) + \frac{\mathcal{M}_{\mp}}{\mathcal{N}} P_{-}(z, z'|\mathbf{q}), \tag{20}$$

$$\Gamma_{\mp\pm}(z, z'|\mathbf{q}) = \frac{3}{2\mathcal{N} l_{tr} l_{\mathrm{dep}}}[P_{-}(z, z'|\mathbf{q}) - P_{+}(z, z'|\mathbf{q})], \tag{21}$$

where

$$\mathcal{M}_{\pm} = \frac{\mathcal{N}}{2} \pm 2(\mathbf{qh}),$$

$$\mathcal{N} = \mathrm{sign}(\mathbf{qh})\sqrt{\left(\frac{3}{l_{tr} l_{\mathrm{dep}}}\right)^2 + 16(\mathbf{qh})^2} \tag{22}$$

and the functions $P_{\pm}(z, z'|\mathbf{q})$ are subject to two independent diffusion equations

$$\left(-\frac{\partial^2}{\partial z^2} + \gamma_{\pm}^2\right) P_{\pm}(z, z'|\mathbf{q}) = \frac{3}{l_{tr}}\delta(z - z') \tag{23}$$

$$\gamma_{\pm}^2 = q^2 + h^2 + \frac{3}{2 l_{tr} l_{\mathrm{dep}}} \pm \frac{\mathcal{N}}{2} \tag{24}$$

with the boundary conditions

$$P_{\pm}(z = -z_0, z'|\mathbf{q}) = P_{\pm}(z = L + z_0, z'|\mathbf{q}) = 0, \tag{25}$$

where L is the thickness of the sample, $z_0 = 0.71 l_{tr}$ is the extrapolated length [16,47].

From Eqs. (9), (13), (20), and (21) it follows that the angular profile of CBS of polarized light from a Faraday medium can be expressed in terms of the intensity found previously in the scalar case [3,4,14–16]. Substituting Eqs. (20) and (21) into Eqs. (9) and (13), we can present the angular profile of CBS in the form

$$\begin{aligned} J_{ij}^{(c)}(\mathbf{q}) = \frac{1}{\mathcal{N}}\Big[\Big[\mathcal{M}_{+} J_{\mathrm{scal}}^{(c)}(\gamma_{+}) + \mathcal{M}_{-} J_{\mathrm{scal}}^{(c)}(\gamma_{-})\Big]\rho_{ij}^{(++)} \\ + \frac{3}{2 l_{tr} l_{\mathrm{dep}}}\Big[J_{\mathrm{scal}}^{(c)}(\gamma_{-}) - J_{\mathrm{scal}}^{(c)}(\gamma_{+})\Big][\rho_{ij}^{(+-)} + \rho_{ij}^{(-+)}] \\ + \Big[\mathcal{M}_{-} J_{\mathrm{scal}}^{(c)}(\gamma_{+}) + \mathcal{M}_{+} J_{\mathrm{scal}}^{(c)}(\gamma_{-})\Big]\rho_{ij}^{(--)}\Big], \end{aligned} \tag{26}$$

where $J_{\mathrm{scal}}^{(c)}(\gamma)$ is the angular profile of CBS within the scalar theory. For example, in the case of backscattering from a semi-infinite medium $J_{\mathrm{scal}}^{(c)}(\gamma)$ is given by the well-known relation [3,4,14–16]

$$J_{\mathrm{scal}}^{(c)}(\gamma) = \frac{3}{8\pi}\frac{1}{(1 + \gamma l_{tr})^2}\left[1 + \frac{1}{\gamma l_{tr}}(1 - e^{-2\gamma z_0})\right], \tag{27}$$

where $\gamma = q$ for a medium with no absorption. The CBS angular profile for a slab of finite thickness L is determined by

$$J_{\mathrm{scal}}^{(c)}(\gamma) = \frac{1}{8\pi\gamma l_{tr}}\frac{1}{\sinh\gamma(L + 2z_0)}$$

$$\times\left[\frac{\cosh\gamma(L+2z_0)-\gamma l_{tr}\sinh\gamma(L+2z_0)}{1-\gamma^2 l_{tr}^2}-\frac{\left(1+\gamma^2 l_{tr}^2\right)\cosh\gamma L-2\gamma l_{tr}\sinh\gamma L}{\left(1-\gamma^2 l_{tr}^2\right)^2}\right]. \quad (28)$$

Equation (28) becomes Eq. (27) in the limit $\gamma \gg 1/L$.

In the most important cases of circularly and linearly polarized incident waves, Eq. (26) gives the following results. For circularly polarized light, CBS occurs only in the helicity-preserving channel, and the CBS intensity is determined by

$$J_{\pm\pm}^{(c)}(\mathbf{q})=\frac{1}{\mathcal{N}}\left[\mathcal{M}_{\pm}J_{\rm scal}^{(c)}(\gamma_+)+\mathcal{M}_{\mp}J_{\rm scal}^{(c)}(\gamma_-)\right], \quad (29)$$

where the upper signs refer to positive helicity, while the lower ones to negative helicity. The CBS intensity in the opposite helicity channel is governed by short wave paths [39] and is always small for Mie scatterers (see, e.g., Refs. [20,39,41]). In our two-mode approximation, it is equal to zero.

For linearly polarized light, the CBS signal can be observed in both co- and cross-polarized channels. The intensities of co- and cross-polarized light are determined by the first and second diagonal elements of matrix (26), respectively,

$$J_{\parallel,\perp}^{(c)}(\mathbf{q})=\frac{1}{4}\left[\left(J_{\rm scal}^{(c)}(\gamma_+)+J_{\rm scal}^{(c)}(\gamma_-)\right)\pm\left(\frac{3}{l_{tr}l_{\rm dep}}\right)\frac{1}{\mathcal{N}}\left(J_{\rm scal}^{(c)}(\gamma_-)-J_{\rm scal}^{(c)}(\gamma_+)\right)\right]. \quad (30)$$

From Eq. (30) it follows that the degree of linear polarization and the total intensity in the CBS cone are equal to

$$P_L=\frac{J_{\parallel}^{(c)}-J_{\perp}^{(c)}}{J_{\parallel}^{(c)}+J_{\perp}^{(c)}}=\left(\frac{3}{l_{tr}l_{\rm dep}}\right)\frac{1}{\mathcal{N}}\frac{J_{\rm scal}^{(c)}(\gamma_-)-J_{\rm scal}^{(c)}(\gamma_+)}{J_{\rm scal}^{(c)}(\gamma_-)+J_{\rm scal}^{(c)}(\gamma_+)} \quad (31)$$

$$J_{\rm tot}^{(c)}(\mathbf{q})=\tfrac{1}{2}\left(J_{\rm scal}^{(c)}(\gamma_+)+J_{\rm scal}^{(c)}(\gamma_-)\right). \quad (32)$$

In CBS from a Faraday medium, the incident linearly polarized light acquires circular polarization. This is due to the Faraday phase shift between interfering time-reversed waves. The intensity of backscattered waves with a given helicity is two times less than that given by Eq. (29),

$$J_{\pm}^{(c)}(\mathbf{q})=\frac{1}{2\mathcal{N}}\left[\mathcal{M}_{\pm}J_{\rm scal}^{(c)}(\gamma_+)+\mathcal{M}_{\mp}J_{\rm scal}^{(c)}(\gamma_-)\right]. \quad (33)$$

The degree of circular polarization is determined by

$$P_C=\frac{J_{+}^{(c)}-J_{-}^{(c)}}{J_{+}^{(c)}+J_{-}^{(c)}}=\frac{\mathcal{M}_{-}-\mathcal{M}_{+}}{\mathcal{N}}\frac{J_{\rm scal}^{(c)}(\gamma_-)-J_{\rm scal}^{(c)}(\gamma_+)}{J_{\rm scal}^{(c)}(\gamma_-)+J_{\rm scal}^{(c)}(\gamma_+)} \quad (34)$$

and arises only in a magnetic field. In the absence of a magnetic field, Eqs. (29)–(33) are transformed into the results obtained previously [39].

B. Angular profile of CBS in magnetic field normal to the surface

In the case of the field directed along the z axis, $\mathbf{h}_{\parallel}=0$ (the Faraday geometry, see, e.g., Refs. [9,45]), Eq. (14) for $\Gamma_{\alpha\beta}(z,z'|\mathbf{q})$, in contrast to the case considered in Sec. III A, cannot be reduced to two independent equations for linear combinations of the elements $\Gamma_{\alpha\beta}(z,z'|\mathbf{q})$. To solve Eq. (14) we represent the solution as the sum of a particular solution of the inhomogeneous equation and the general solution of the homogeneous equation.

The particular solution of Eq. (14) has the form

$$\Gamma_{\pm\pm}^{(\rm part)}(z,z'|\mathbf{q})=\frac{3}{4l_{tr}}\left[\frac{e^{-\gamma_-|z-z'|}}{\gamma_-}\left(1+\frac{4h^2}{\gamma_+^2-\gamma_-^2}\right)+\frac{e^{-\gamma_+|z-z'|}}{\gamma_+}\left(1-\frac{4h^2}{\gamma_+^2-\gamma_-^2}\right)\pm\frac{4ih\,\mathrm{sign}(z-z')}{\gamma_+^2-\gamma_-^2}\times\left(e^{-\gamma_-|z-z'|}-e^{-\gamma_+|z-z'|}\right)\right] \quad (35)$$

$$\Gamma_{-+}^{(\rm part)}(z,z'|\mathbf{q})=\Gamma_{+-}^{(\rm part)}(z,z'|\mathbf{q})=\frac{9}{4l_{tr}^2 l_{\rm dep}}\frac{1}{(\gamma_+^2-\gamma_-^2)}\left[\frac{e^{-\gamma_-|z-z'|}}{\gamma_-}-\frac{e^{-\gamma_+|z-z'|}}{\gamma_+}\right], \quad (36)$$

where

$$\gamma_{\pm}^2=\left(q^2+\frac{3}{2l_{tr}l_{\rm dep}}\right)-h^2\pm\sqrt{\left(\frac{3}{2l_{tr}l_{\rm dep}}\right)^2-4h^2\left(q^2+\frac{3}{2l_{tr}l_{\rm dep}}\right)}. \quad (37)$$

For a slab of finite thickness, the general solution of the corresponding homogeneous equation proves to be cumbersome. We present here a solution to the problem for a semi-infinite medium. The general solution of the homogeneous equation [i.e., Eq. (14) without a source on the right-hand side] can be written as

$$\Gamma_{\pm+}^{(\rm gen)}(z,z'|\mathbf{q})=\mathcal{A}_{\pm}^{(-)}e^{-\gamma_-(z+z'+2z_0)}+\mathcal{A}_{\pm}^{(+)}e^{-\gamma_+(z+z'+2z_0)}+\mathcal{B}_{\pm}^{(+)}e^{-\gamma_- z-\gamma_+ z'+(\gamma_-+\gamma_+)z_0}+\mathcal{B}_{\pm}^{(-)}e^{-\gamma_+ z-\gamma_- z'+(\gamma_-+\gamma_+)z_0}. \quad (38)$$

The coefficients $\mathcal{A}_{\pm}^{(\pm)}$ and $\mathcal{B}_{\pm}^{(\pm)}$ appearing in Eq. (38) are determined from the homogeneous equation itself and the boundary condition

$$\left(\Gamma_{\pm+}^{(\rm part)}(z,z'|\mathbf{q})+\Gamma_{\pm+}^{(\rm gen)}(z,z'|\mathbf{q})\right)|_{z=-z_0}=0. \quad (39)$$

The values of the coefficients are equal to

$$\mathcal{A}_{+}^{(\pm)}=-\frac{(\gamma_\pm-ih)^2-(\gamma_\mp+ih)^2}{(\gamma_\pm+ih)^2-(\gamma_\mp+ih)^2}\,\mathcal{R}^{(\pm)}$$

$$\mathcal{B}_{+}^{(\pm)}=-\frac{4ih\gamma_\pm}{(\gamma_\pm+ih)^2-(\gamma_\mp+ih)^2}\,\mathcal{R}^{(\pm)}, \quad (40)$$

where

$$\mathcal{R}^{(\pm)}=\frac{3}{l_{tr}}\left(\frac{1}{4\gamma_\pm}+\frac{ih}{\gamma_\pm^2-\gamma_\mp^2}-\frac{h^2}{\gamma_\pm(\gamma_\pm^2-\gamma_\mp^2)}\right) \quad (41)$$

and

$$\mathcal{A}_{-}^{(\pm)}=-\frac{9}{4l_{tr}^2 l_{\rm dep}}\frac{1}{\gamma_\pm(\gamma_\mp^2-\gamma_\pm^2)}\frac{(\gamma_\pm+ih)^2-(\gamma_\mp-ih)^2}{(\gamma_\pm-ih)^2-(\gamma_\mp-ih)^2}$$

$$\mathcal{B}_{-}^{(\pm)}=-\frac{9}{l_{tr}^2 l_{\rm dep}(\gamma_\pm^2-\gamma_\mp^2)}\frac{ih}{(\gamma_\pm-ih)^2-(\gamma_\mp-ih)^2}. \quad (42)$$

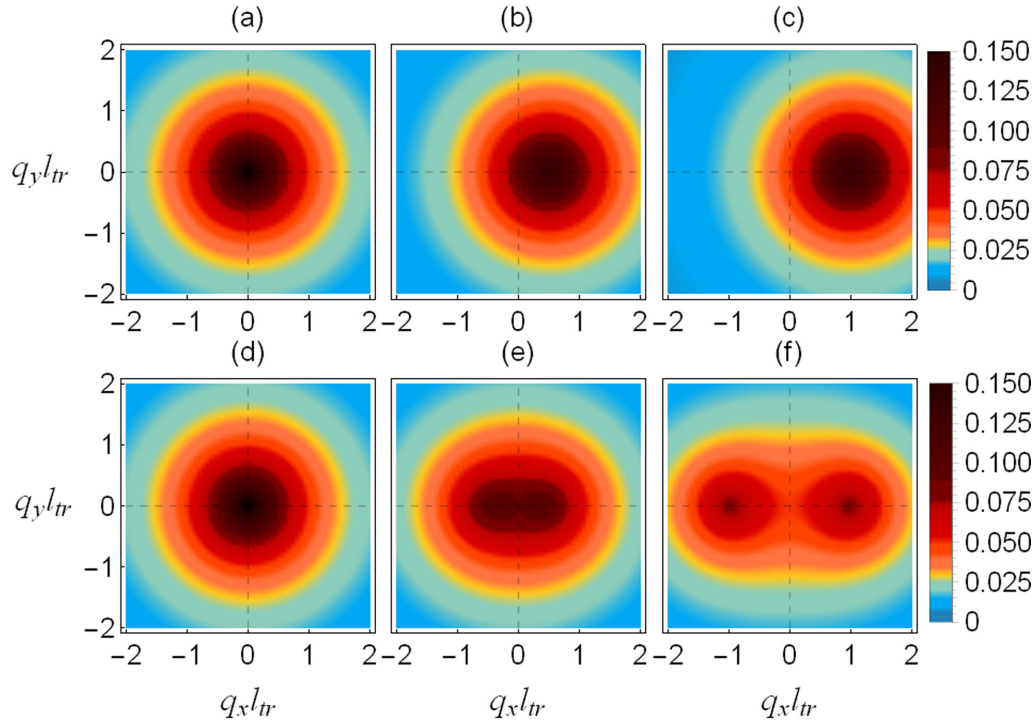

FIG. 3. Intensity distribution in the CBS cone for circularly and linearly polarized light [$hl_{tr} = 0$ (a) and (d), 0.5 (b) and (e), 1.0 (c) and (f), $\sigma_{\rm dep}/\sigma_{tr} = 0.1$].

Substituting Eqs. (35), (36), and (38) into Eq. (9) we find the expressions for the elements of $J^{(c)}_{\alpha\beta}(\mathbf{q}) = J^{(\rm part)}_{\alpha\beta}(\mathbf{q}) + J^{(\rm gen)}_{\alpha\beta}(\mathbf{q})$, where

$$J^{(\rm part)}_{++}(\mathbf{q}) = \frac{3}{16\pi} \times \left[\frac{1}{\gamma_- l_{tr}}\left(1 - \frac{4h^2}{\gamma_-^2 - \gamma_+^2}\right)\frac{1+\gamma_- l_{tr}}{(1+\gamma_- l_{tr})^2 + h^2 l_{tr}^2} + \frac{1}{\gamma_+ l_{tr}}\left(1 - \frac{4h^2}{\gamma_+^2 - \gamma_-^2}\right)\frac{1+\gamma_+ l_{tr}}{(1+\gamma_+ l_{tr})^2 + h^2 l_{tr}^2} - \frac{4h^2}{\gamma_-^2 - \gamma_+^2}\frac{1}{(1+\gamma_- l_{tr})^2 + h^2 l_{tr}^2} - \frac{4h^2}{\gamma_+^2 - \gamma_-^2}\frac{1}{(1+\gamma_+ l_{tr})^2 + h^2 l_{tr}^2}\right] \tag{43}$$

$$J^{(\rm part)}_{-+}(\mathbf{q}) = \frac{9}{16\pi l_{tr}^2 l_{\rm dep}(\gamma_+^2 - \gamma_-^2)}\frac{1}{1+ihl_{tr}} \times \left[\frac{1}{\gamma_-}\frac{1}{1+\gamma_- l_{tr} + ihl_{tr}} - \frac{1}{\gamma_+}\frac{1}{1+\gamma_+ l_{tr} + ihl_{tr}}\right] \tag{44}$$

$$J^{(\rm gen)}_{++}(\mathbf{q}) = \frac{1}{4\pi}\left[\frac{\mathcal{A}_+^{(-)} e^{-2\gamma_- z_0}}{(1+\gamma_- l_{tr})^2 + h^2 l_{tr}^2} + \frac{\mathcal{A}_+^{(+)} e^{-2\gamma_+ z_0}}{(1+\gamma_+ l_{tr})^2 + h^2 l_{tr}^2} + \frac{\mathcal{B}_+^{(+)} e^{-(\gamma_- + \gamma_+) z_0}}{(1+ihl_{tr} + \gamma_- l_{tr})(1 - ihl_{tr} + \gamma_+ l_{tr})} + \frac{\mathcal{B}_+^{(-)} e^{-(\gamma_- + \gamma_+) z_0}}{(1+ihl_{tr} + \gamma_+ l_{tr})(1 - ihl_{tr} + \gamma_- l_{tr})}\right] \tag{45}$$

$$J^{(\rm gen)}_{-+}(\mathbf{q}) = \frac{1}{4\pi}\left[\frac{\mathcal{A}_-^{(-)} e^{-2\gamma_- z_0}}{(1+ihl_{tr} + \gamma_- l_{tr})^2} + \frac{\mathcal{A}_-^{(+)} e^{-2\gamma_+ z_0}}{(1+ihl_{tr} + \gamma_+ l_{tr})^2} + \frac{(\mathcal{B}_-^{(-)} + \mathcal{B}_-^{(+)}) e^{-(\gamma_- + \gamma_+) z_0}}{(1+ihl_{tr} + \gamma_- l_{tr})(1+ihl_{tr} + \gamma_+ l_{tr})}\right]. \tag{46}$$

The corresponding expressions for $\Gamma^{(\rm gen)}_{\mp-}(z, z'|\mathbf{q})$ and $J^{(c)}_{\pm-}(\mathbf{q})$ differ from those for $\Gamma^{(\rm gen)}_{\pm+}(z, z'|\mathbf{q})$ and $J^{(c)}_{\pm+}(\mathbf{q})$ only by changing the sign of h.

IV. DISCUSSION AND COMPARISON WITH EXPERIMENT

The effects accompanying CBS in the magnetic field parallel to the sample surface $\mathbf{H} = (H, 0, 0)$ are illustrated in Figs. 3–6 for two cases of the incident light polarization. For a circularly polarized beam incident on the sample, the CBS cone is shifted from the exact backward direction [see Figs. 3(a)–3(c)] and blunted as the magnetic field increases. The CBS angular profiles for $\mathbf{q}$ parallel to $\mathbf{h}$ are shown in Fig. 4 depending on the magnetic field strength and the ratio of the helicity-flip scattering cross section to the transport scattering one, $\sigma_{\rm dep}/\sigma_{tr}$. From the results presented it follows that the greater the ratio $\sigma_{\rm dep}/\sigma_{tr}$, the more the magnetic field suppresses the CBS. For $\mathbf{q}$ perpendicular to $\mathbf{h}$, the

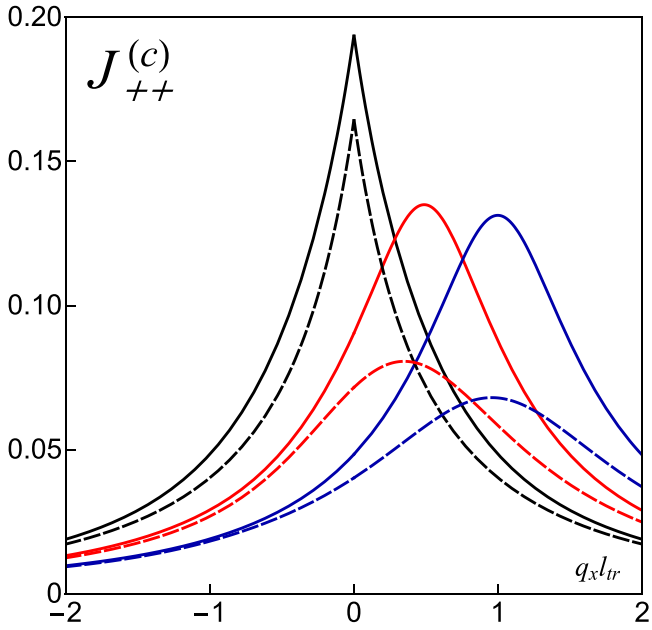

FIG. 4. Angular profile of CBS intensity in the helicity-preserving channel. The magnetic field is parallel to the sample surface [from left curves to right ones $hl_{tr} = 0$, 0.5 and 1, $\sigma_{\rm dep}/\sigma_{tr} =$ 0.1 (solid curves) and 0.5 (dashed curves)].

magnetic field effect is reduced only to blunting the CBS angular profile.

For high-order scattering events, the probability of scattering with helicity flip becomes great. In its turn, helicity-flip scattering leads to the appearance of waves with opposite helicity, the interference between which is destroyed by the magnetic field. Therefore, the high-order scattering contribution to the CBS intensity is suppressed, resulting in the CBS peak blunting in the magnetic field.

According to Eq. (29), in the strong magnetic field, $h \gg (l_{tr} l_{\rm dep})^{-1/2}$, the CBS angular profile tends to a universal form,

$$J^{(c)}_{\pm\pm}(\mathbf{q}) = J^{(c)}_{\rm scal}\left(\sqrt{(\mathbf{q} \mp \mathbf{h})^2 + 3/(2 l_{tr} l_{\rm dep})}\right). \qquad (47)$$

Note that a shift of the CBS peak similar to that discussed above was predicted previously for electrons [35] where it is a manifestation of the Aharonov-Bohm effect and is due to a nonzero average phase shift between interfering electron waves.

For a linearly polarized beam incident on the sample, the CBS cone splits into two ones [see Figs. 3(d)–3(f)]. The peaks move apart and smooth out as the magnetic field increases. This is valid for both co- and cross-polarization channels (see Fig. 5). In addition, the light within the CBS cone acquires circular polarization [see Eq. (34)], the degree of which increases with magnetic field strength. Aforesaid is illustrated in Fig. 6. For $\mathbf{q}$ perpendicular to $\mathbf{h}$, the CBS angular profile is qualitatively the same as that obtained for the circularly polarized beam.

In the strong magnetic field, the angular profiles for both polarizations coincide with each other and, according to

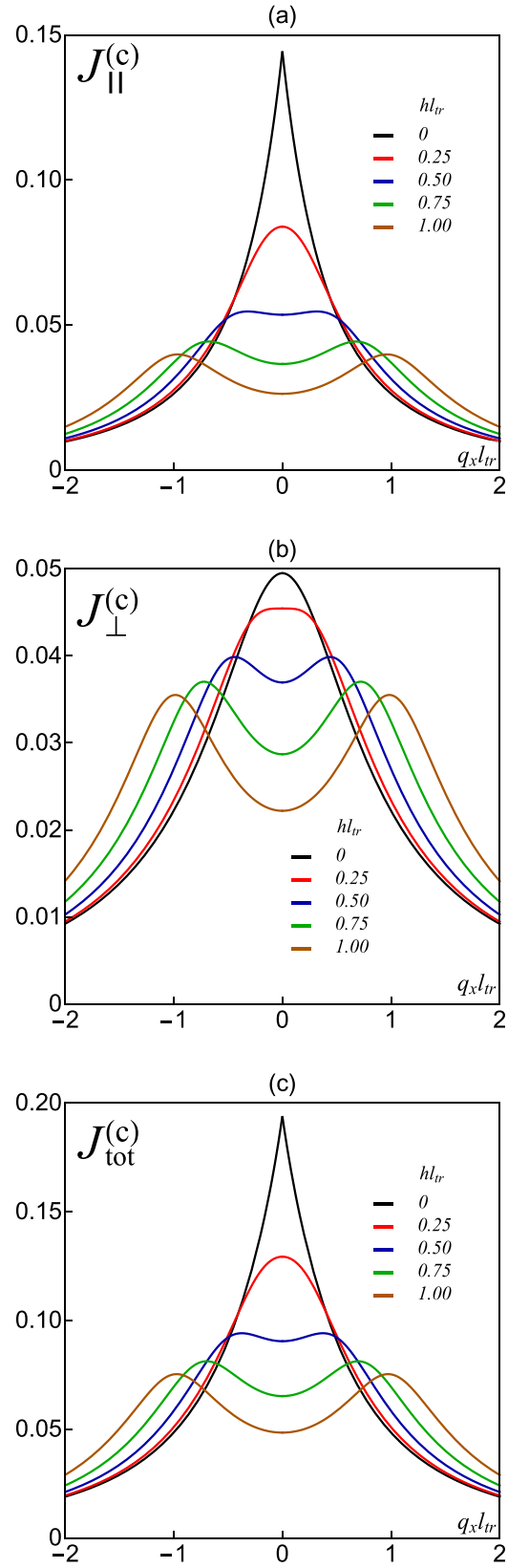

FIG. 5. Angular profiles of CBS intensity for linearly copolarized (a) and cross-polarized (b) backscattered light, the total intensity is shown in (c). The magnetic field is parallel to the sample surface (from top curves to bottom ones, $hl_{tr} = 0$, 0.25, 0.5, 0.75, 1, $\sigma_{\rm dep}/\sigma_{tr} = 0.1$).

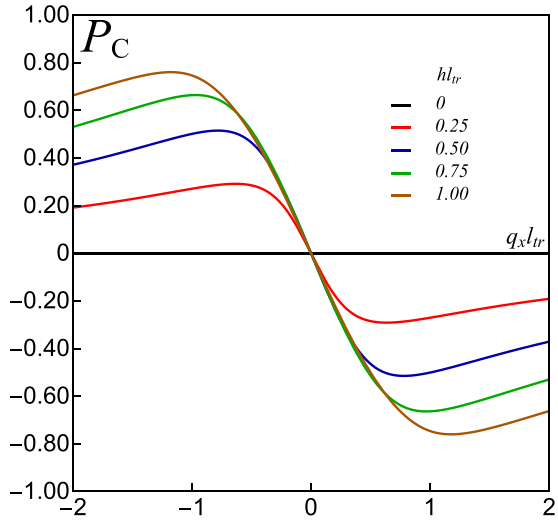

FIG. 6. Degree of circular polarization in backscattering of linearly polarized light. The magnetic field is parallel to the sample surface (from bottom curves to top ones for $\mathbf{qh} > 0$, $hl_{tr} = 0, 0.25, 0.5, 0.75, 1$, $\sigma_{\rm dep}/\sigma_{tr} = 0.1$).

Eq. (30), take the form

$$J^{(c)}_{\parallel,\perp}(\mathbf{q}) = \tfrac{1}{4}\big[J^{(c)}_{\rm scal}(\sqrt{(\mathbf{q}-\mathbf{h})^2 + 3/(2l_{tr}l_{\rm dep})}) + J^{(c)}_{\rm scal}(\sqrt{(\mathbf{q}+\mathbf{h})^2 + 3/(2l_{tr}l_{\rm dep})})\big]. \quad (48)$$

From Eqs. (47) and (48) it follows that the strong magnetic field controls only the CBS peak position, while the width of the angular profile is governed by the rate of light depolarization.

In the magnetic field perpendicular to the sample surface, the main effect is in blunting the CBS angular profile with increasing field strength. Such a behavior is inherent in both circular and linear initial polarization of light (see Fig. 7). Besides, for linearly polarized light incident on the sample, both circular polarization and turn of the initial polarization plane should be observed in the CBS cone. The latter effect is determined by the third Stokes parameter $U = \mathrm{Im}\,(J^{(c)}_{-+} - J^{(c)}_{+-})/2$ and is the result of the Faraday rotation along the part of a wave path of the order of l_{tr}.

In the limit of the strong magnetic field the values of $\gamma_\pm$ [see Eq. (37)] tend to $\gamma_\pm = \sqrt{q^2 + 3/(2l_{tr}l_{\rm dep})} \pm ih$ and the CBS angular profile ceases to depend on the magnetic field. In the case of circular initial polarization, the angular profile is given by

$$J^{(c)}_{\pm\pm}(\mathbf{q}) = J^{(c)}_{\rm scal}(\sqrt{q^2 + 3/(2l_{tr}l_{\rm dep})}). \quad (49)$$

For a linearly polarized beam, the angular profiles of backscattered light in co- and cross-polarized channels are coincident with each other and equal to half the intensity (49). This correlates well with the inference drawn previously from Monte Carlo simulation [20]. Comparison of our results with Monte Carlo simulation data [20] is illustrated in Fig. 8, which shows the dependence of the CBS intensity in the exact backward direction on the magnetic field strength.

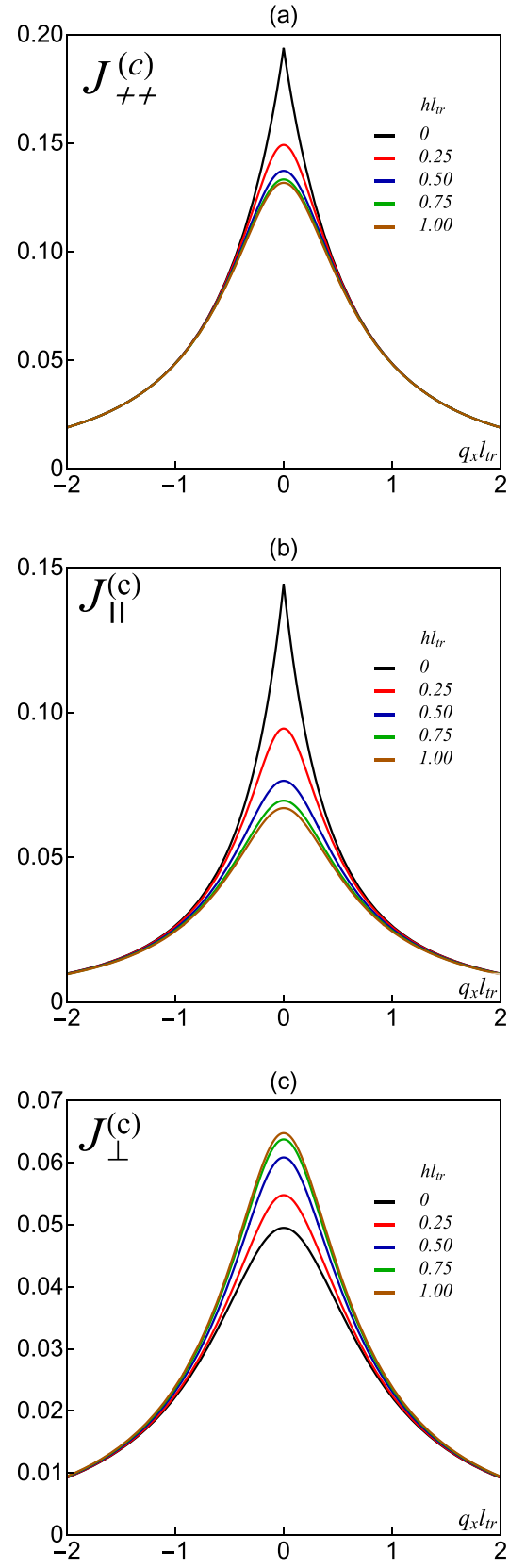

FIG. 7. Angular profiles of CBS intensity for the helicity-preserving channel (a) and for linearly copolarized (b) and cross-polarized (c) backscattered light. The magnetic field is perpendicular to the sample surface (from top to bottom curves in (a) and (b) and vice versa in (c) $hl_{tr} = 0, 0.25, 0.5, 0.75, 1$, $\sigma_{\rm dep}/\sigma_{tr} = 0.1$).

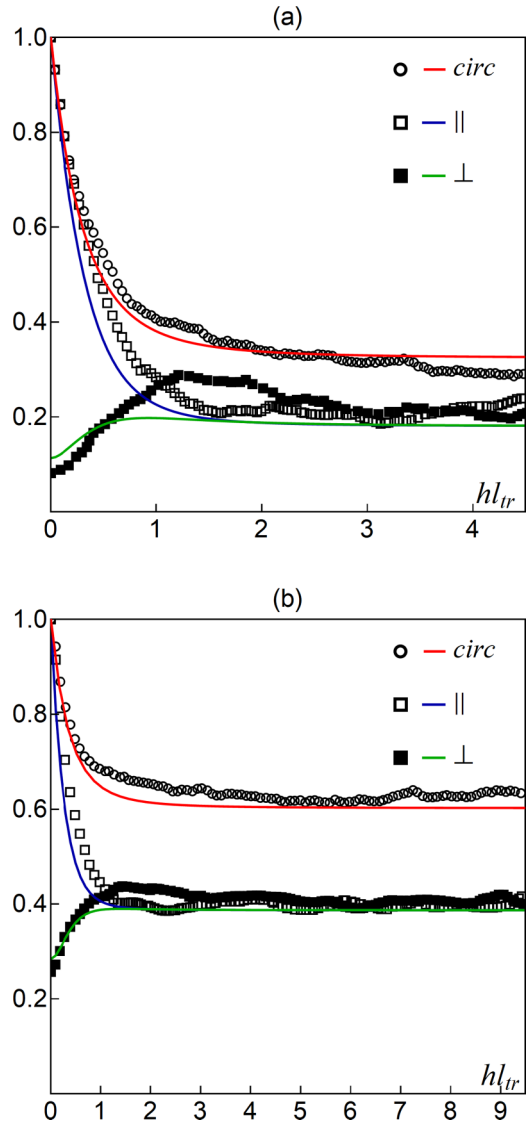

FIG. 8. Interference contribution to intensity in the exact backward direction for circularly polarized light (helicity preserving channel, top solid curve) and for linearly co- and cross-polarized light (two bottom curves, respectively) as a function of magnetic field strength. The curves are normalized to unity at $\mathbf{H} = 0$ (cross-polarized contribution is normalized to the value of copolarized one at $\mathbf{H} = 0$). The results of Monte Carlo simulation [20] are shown by symbols. The results presented refer to the samples containing Mie spheres (the relative refractive index $n = 0.858$, (a) size parameter $ka = 2.32$, $\sigma_{\rm dep}/\sigma_{tr} = 0.68$ and (b) size parameter $ka = 23.2$, $\sigma_{\rm dep}/\sigma_{tr} = 0.15$), the sample transport optical thickness is $L/l_{tr} = 15$. The magnetic field is perpendicular to the sample surface.

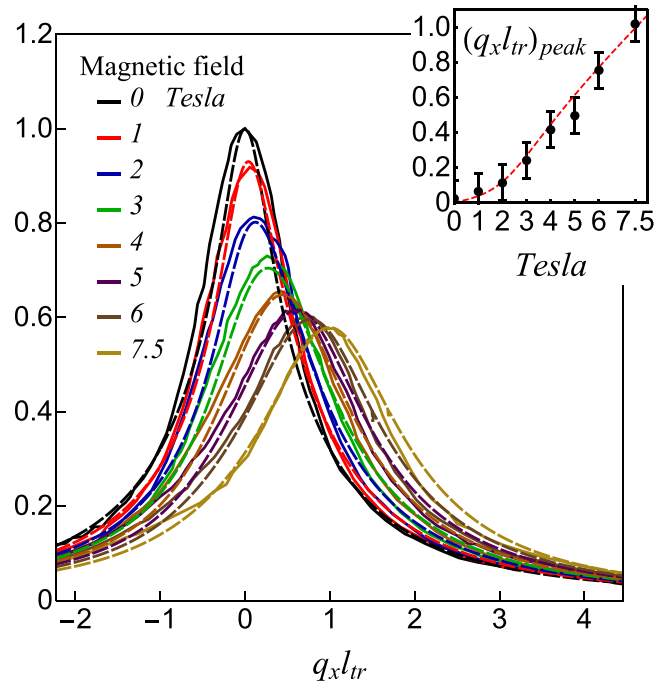

FIG. 9. Comparison of the CBS angular profiles measured in experiment [27] (solid curves) and calculated with Eq. (29) (dashed curves) for the helicity-preserving channel. The magnetic field is parallel to the surface, its values are shown in the legend to the figure (the corresponding values of parameter hl_{tr} are 0, 0.14, 0.27, 0.41, 0.54, 0.68, 0.82, and 1.02). The angular profiles are normalized to the intensity in the exact backward direction at $h = 0$. The calculations were performed for the same values of the sample thickness L and the transport mean-free path l_{tr} as in Ref. [27], $L = 3.5$ mm and $l_{tr} = 445$ μm, respectively, $\sigma_{\rm dep}/\sigma_{tr} = 0.47$. The displacement of the CBS peak from the backward direction as a function of the magnetic field is shown in the inset (symbols are experimental data [27], dashed curve is our result).

The asymptotic results (47)–(49) reflect the fact that the magnetic field does not violate wave interference on paths shorter than the mean-free path relative to helicity-flip collisions. On such paths, the contribution from waves that change their helicity [exactly these waves are responsible for the difference between $J_{\parallel}^{(c)}$ and $J_{\perp}^{(c)}$, see Eq. (16)] does not arise.

Note that in the absence of helicity-flip scattering, the magnetic field does not disturb the wave interference at all. Such a situation can be realized under the first Kerker condition [48] (see also Refs. [31,32]), where the helicity-flip scattering cross section is extremely small and the ratio $\sigma_{\rm dep}/\sigma_{tr}$ can achieve values of the order of a few hundredths.

In the opposite case, where every scattering event is accompanied by a random change in the helicity of light, $\sigma_{\rm dep}/\sigma_{tr} \sim 1$, the CBS features discussed above disappear, and the effect of the magnetic field is reduced only to suppression of wave interference [17–19]. For Rayleigh scattering, this is shown in Appendix B.

The results obtained above [see, e.g., Eqs. (29) and (30)] enable explaining the experimental data of Ref. [27]. In the experiment [27] the dependence of the CBS angular profile on the magnetic field strength were measured for circularly and linearly polarized light backscattered from a porous magnetoactive glass. The magnetic field was oriented parallel to the sample surface. Comparison of the results of our calculations with the data of Ref. [27] is shown in Figs. 9 and 10. When comparing with the experimental data, we did not use any fitting parameters. The ratio $\sigma_{\rm dep}/\sigma_{tr}$ was calculated with the Mie theory for the optical characteristics of the magnetoactive glass taken from Ref. [27]. The CBS angular profiles shown

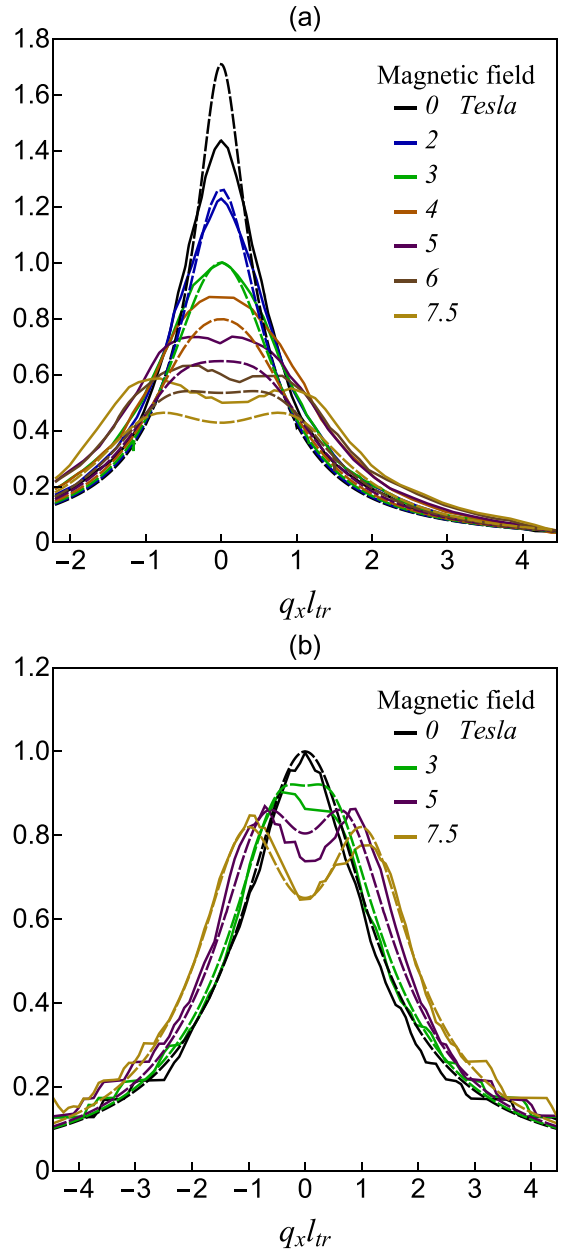

FIG. 10. Comparison of the CBS angular profiles measured in experiment [27] (solid curves) and calculated with Eq. (30) (dashed curves) for linearly polarized light. The polarization of backscattered light is (a) coincident or (b) orthogonal to the polarization of the incident light. The other parameters are the same as in the Fig. 9.

in Figs. 9 and 10(b) are normalized to the value of the corresponding backscattering intensity $I(\mathbf{q} = 0, \mathbf{h} = 0)$. In the case of linear polarization of the incident beam, the CBS angular profiles for copolarized light [see Fig. 10(a)] are normalized to the backscattering intensity at magnetic field of 2 Tesla ($hl_{tr} = 0.27$) [27], since the peak of the experimental angular profile at $\mathbf{H} = 0$ is rather smoothed, which makes it difficult reproducing the $\mathbf{H}$ dependence of the intensity value. Good agreement between our results and experiment [27] indicates the key role of helicity-flip scattering process in manipulating the interference of time-reversed waves in a magnetic field.

V. CONCLUSIONS

In conclusion, we have studied coherent backscattering (CBS) of light from a disordered ensemble of Mie particles embedded in a magnetoactive medium. We have shown that the reason for suppression of coherent backscattering of light in a magnetic field is not the Faraday effect itself, but the helicity-flip scattering events leading to the appearance of waves with opposite helicity. The Faraday effect suppresses the interference of waves with opposite helicity, but does not destroy the interference of time-reversed waves with identical helicity.

We have developed the CBS diffusion theory, which takes into account both the Faraday effect and the effect of circular polarization memory specific to Mie scattering. The theory is based on a system of coupled diffusion equations for two cooperon modes responsible for the interference of waves with identical helicity. The interaction between cooperons is due to the helicity-flip scattering. Under conditions of the circular polarization memory effect, the ratio of the helicity-flip scattering cross section to the transport scattering one is small. Analytical expressions for the CBS angular profile have been derived for the magnetic field oriented parallel and perpendicular to the sample surface and for different polarization states of the incident and backscattered light. The results obtained have enabled explaining the unusual features found in Monte Carlo simulation and in experiment on light scattering by Mie spheres in magnetoactive glass [20,22,27], in particular, a displacement and splitting of the CBS peak depending on the polarization state of the incident light, as well as the saturation of the magnetic field dependence of the CBS intensity. In the limit of Rayleigh scattering, our results are transformed into those derived in Refs. [17,19].

The results obtained above present a theoretical groundwork for studies of the interaction of electromagnetic waves with magnetoactive disordered materials, and can also be of interest for the development of experimental methods for quantifying their optical characteristics (e.g., the Verdet constant [12,34]).

ACKNOWLEDGMENTS

This work was partially supported by the MEPhI Program "Priority-2030".

APPENDIX A: SYSTEM OF DIFFUSION EQUATIONS FOR COOPERON

The sum of ladder diagrams $\langle G(\mathbf{h})G^*(-\mathbf{h})\rangle_L$, via which the sum of the most-crossed diagrams $\langle G(\mathbf{h})G^*(\mathbf{h})\rangle_C$ is expressed [see Eq. (6)], obeys the equation shown in Fig. 11 [17–19]. Following Ref. [18] we can transform this diagrammatic equation to the transport equation in the integral form. Going to the fast and slow variables $\mathbf{\Delta} = \mathbf{r} - \mathbf{r}'$ and $\mathbf{R} = (\mathbf{r} + \mathbf{r}')/2$ and assuming

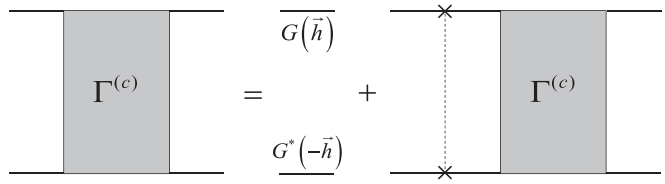

FIG. 11. Integral equation for the sum of ladder diagrams $\langle G(\mathbf{h})G^*(-\mathbf{h})\rangle_L$.

that the characteristic scales of their change differ greatly, $\Delta \sim k_0^{-1} \ll R \sim l$ ($\Delta/R \sim 1/k_0 l \ll 1$, l is the mean-free path), we represent the product of the Green's functions as follows:

$$\left\langle G_{ik}\left(\mathbf{R}+\frac{\mathbf{\Delta}}{2},\mathbf{R}'+\frac{\mathbf{\Delta}'}{2}\middle|\mathbf{h}\right)\right\rangle\left\langle G^*_{lm}\left(\mathbf{R}-\frac{\mathbf{\Delta}}{2},\mathbf{R}'-\frac{\mathbf{\Delta}'}{2}\middle|-\mathbf{h}\right)\right\rangle$$
$$=\frac{e^{-|\mathbf{R}-\mathbf{R}'|/l}}{|\mathbf{R}-\mathbf{R}'|^2}\,e^{ik_0\mathbf{n}\mathbf{\Delta}-ik_0\mathbf{n}'\mathbf{\Delta}'}\sum_{\alpha,\beta}P^{(\alpha)}_{ik}(\mathbf{n})P^{(\beta)}_{ml}(\mathbf{n})\exp\left(-i\mathbf{h}\cdot(\mathbf{R}-\mathbf{R}')\left(\frac{\alpha+\beta}{2}\right)\right), \tag{A1}$$

where $\mathbf{n}=(\mathbf{R}-\mathbf{R}')/|\mathbf{R}-\mathbf{R}'|$, α and β denote the helicity and equal ±1 [see Eq. (1)]. Further performing the Fourier transform with respect to $\mathbf{\Delta}$ we obtain the transport equation for the sum of ladder diagrams $\Gamma^{(c)}=\langle G(\mathbf{h})G^*(-\mathbf{h})\rangle_L$ in the Wigner representation [18]

$$\Gamma^{(c)}_{il,km}(\mathbf{R},\mathbf{n}|\mathbf{R}',\mathbf{n}')=\Gamma^{(0)}_{il,km}(\mathbf{R},\mathbf{n}|\mathbf{R}',\mathbf{n}')+\int d\mathbf{R}_1\int d\mathbf{n}_1\Gamma^{(0)}_{il,i'l'}(\mathbf{R},\mathbf{n}|\mathbf{R}_1,\mathbf{n}_1)\int d\mathbf{n}_2\,d_{i'l',i''l''}(\mathbf{n}_1,\mathbf{n}_2)\Gamma^{(c)}_{i''l'',km}(\mathbf{R}_1,\mathbf{n}_2|\mathbf{R}',\mathbf{n}'), \tag{A2}$$

where $\Gamma^{(0)}_{il,km}$ is expressed in terms of the product of the average Green's functions (A1) in the Wigner representation [18]

$$\Gamma^{(0)}_{il,km}(\mathbf{R},\mathbf{n}|\mathbf{R}',\mathbf{n}')=\delta(\mathbf{n}-\mathbf{n}')\delta\left(\mathbf{n}-\frac{\mathbf{R}-\mathbf{R}'}{|\mathbf{R}-\mathbf{R}'|}\right)\cdot\frac{\exp\left(-|\mathbf{R}-\mathbf{R}'|/l\right)}{|\mathbf{R}-\mathbf{R}'|^2}\cdot$$
$$\sum_{\alpha,\beta}P^{(\alpha)}_{ik}(\mathbf{n})P^{(\beta)}_{ml}(\mathbf{n})\exp\left(-i\mathbf{h}\cdot(\mathbf{R}-\mathbf{R}')\left(\frac{\alpha+\beta}{2}\right)\right), \tag{A3}$$

and $d_{il,km}(\mathbf{n},\mathbf{n}')$ is the scattering matrix [41], which describes single scattering in the medium. The scattering matrix can be expressed in terms of the dielectric constant of scattering particles or the scattering amplitudes [41,49].

Equations (A1)–(A3) are written in the laboratory reference frame (the Cartesian coordinate system with the z axis directed along the inward normal to the sample surface). It is convenient to additionally transform the equation (A2) by going from the laboratory reference frame to the concomitant reference frame associated with the direction $\mathbf{n}$ of propagation (see, e.g., Refs. [18,41]). To do this we take advantage of the basis of three unit vectors $\mathbf{n}=(\sin\theta\cos\varphi,\sin\theta\sin\varphi,\cos\theta)$, $\mathbf{e}^{(\pm)}=(\partial\mathbf{n}/\partial\theta\mp i[\mathbf{n}\times\partial\mathbf{n}/\partial\theta])/\sqrt{2}$, which is known as a circular basis. In the system of the vectors $\mathbf{e}^{(\pm)}$, the electric field can be represented as a superposition of two circularly polarized waves with different helicity [41,50]

$$\mathbf{E}=\mathbf{e}^{(+)}E_+ + \mathbf{e}^{(-)}E_-. \tag{A4}$$

Following [50] we can rewrite this equation in the form $E_i=\sum_\alpha e_i^{(\alpha)}E_\alpha$ where Latin and Greek indices take the values $i=x,y,z$ and $\alpha=+,-$. The unit vectors $\mathbf{e}^{(\pm)}$ are orthogonal to each other, $e_i^{(\alpha)}e_i^{(\beta)}=\delta_{\alpha\beta}$, and subject to the condition of completeness $e_i^{(+)}e_j^{(+)}+e_i^{(-)}e_j^{(-)}+n_in_j=\delta_{ij}$.

According to Eq. (A4) the matrix $\Gamma^{(c)}_{il,km}(\mathbf{R},\mathbf{n}|\mathbf{R}',\mathbf{n}')$ appearing in Eq. (A2) is transformed in going from the laboratory reference frame to the concomitant one as follows:

$$\Gamma^{(c)}_{il,km}(\mathbf{R},\mathbf{n}|\mathbf{R}',\mathbf{n}')=\sum_{\alpha,\beta,\gamma,\delta}e_i^{(\alpha)}(e_l^{(\beta)})^*\Gamma^{(c)}_{\alpha\beta,\gamma\delta}(\mathbf{R},\mathbf{n}|\mathbf{R}',\mathbf{n}')e_k^{(\gamma)}(e_m^{(\delta)})^*. \tag{A5}$$

In conditions of circular polarization (or helicity) memory (see, e.g., Refs. [28–32]), only two slowly decaying modes propagate in the medium. These are the sum of intensities of the waves polarized clockwise and counterclockwise and the difference between them (i.e., the first and fourth Stokes parameters, respectively). The length of attenuation for each of these modes exceeds noticeably the transport mean-free path, which enables applying the diffusion approximation the their calculation [30,39].

Assuming that the helicity memory condition is fulfilled, we can keep in Eq. (A5) only the terms with pairwise coinciding indices, i.e., $\Gamma^{(c)}_{\alpha\alpha,\beta\beta} \equiv \Gamma^{(c)}_{\alpha\beta}$. Then Eq. (A5) reduces to

$$\Gamma^{(c)}_{il,km}(\mathbf{R},\mathbf{n}|\mathbf{R}',\mathbf{n}') = \sum_{\alpha,\beta=+,-} P^{(\alpha)}_{il}(\mathbf{n})\Gamma^{(c)}_{\alpha\beta}(\mathbf{R},\mathbf{n}|\mathbf{R}',\mathbf{n}')P^{(\beta)}_{mk}(\mathbf{n}'). \tag{A6}$$

Substituting Eq. (A6) into Eq. (A2) we obtain the equation for the elements $\Gamma^{(c)}_{\alpha\beta}$. The scattering matrix $d_{\alpha\beta}(\mathbf{nn}')$ appearing in this equation is related to $d_{il,km}(\mathbf{n},\mathbf{n}')$ by the formula

$$d_{\alpha\beta}(\mathbf{nn}') = P^{(\alpha)}_{il}(\mathbf{n})d_{il,km}(\mathbf{n},\mathbf{n}')P^{(\beta)}_{km}(\mathbf{n}'), \tag{A7}$$

where summation over repeated indices is implied. In the case of weak (Born or Rayleigh-Gans [49]) scatterers, the elements $d_{\alpha\beta}$ take the form

$$\begin{aligned} d_{\pm\pm}(\mathbf{nn}') &= \tfrac{1}{4}(1+(\mathbf{nn}'))^2\, n_0|F(\mathbf{nn}')|^2, \\ d_{+-}(\mathbf{nn}') &= d_{-+}(\mathbf{nn}') = \tfrac{1}{4}(1-(\mathbf{nn}'))^2\, n_0|F(\mathbf{nn}')|^2, \end{aligned} \tag{A8}$$

where n_0 is the number of particles per unit volume, and $F(\mathbf{nn}') = (k_0^2/4\pi)\int_V d\mathbf{r}\, e^{ik_0(\mathbf{n}-\mathbf{n}')\mathbf{r}}(\epsilon-1)$, integration is carried out over the volume of the particle. In the case of a continuous random medium, the quantity $n_0|F(\mathbf{nn}')|^2$ appearing in Eq. (A8) should be replaced by $(k_0^4/16\pi^2)\int d\mathbf{r}-\mathbf{r}')\, e^{ik_0(\mathbf{n}-\mathbf{n}')(\mathbf{r}-\mathbf{r}')}\langle\delta\epsilon(\mathbf{r})\delta\epsilon(\mathbf{r}')\rangle$, where $\langle\delta\epsilon\delta\epsilon\rangle$ is the correlation function of the dielectric constant (see, e.g., Ref. [51]). In the case of Mie particles, the matrix $d_{\alpha\beta}(\mathbf{nn}')$ is expressed in terms of the scattering amplitudes for the field components polarized parallel and perpendicularly to the scattering plane, $A_\parallel$ and $A_\perp$, [49]

$$d_{\alpha\beta}(\mathbf{nn}') = n_0 a_{\alpha\beta}(\mathbf{nn}'), \tag{A9}$$

where $a_{\pm\pm}(\mathbf{nn}') = a_+(\mathbf{nn}')$, $a_{\pm\mp}(\mathbf{nn}') = a_-(\mathbf{nn}')$, and $a_\pm(\mathbf{nn}') = |A_\parallel \pm A_\perp|^2/4$ (see also Ref. [42]). The elements $a_{\alpha\beta}(\mathbf{nn}')$ can also be represented as linear combinations of elements $a_1(\mathbf{nn}')$ and $a_2(\mathbf{nn}')$ of the conventional scattering matrix used in the radiative transfer theory [41,42,47], $a_\pm(\mathbf{nn}') = [a_1(\mathbf{nn}') \pm a_2(\mathbf{nn}')]/2$.

Acting on both sides of the integral equation for $\Gamma^{(c)}_{\alpha\beta}(\mathbf{R},\mathbf{n}|\mathbf{R}',\mathbf{n}')$ by the operator

$$\left[\left\{\mathbf{n}\frac{\partial}{\partial\mathbf{R}} + \frac{1}{l}\right\}\delta_{\alpha\beta} + i(\mathbf{nh})(\hat{\sigma}_z)_{\alpha\beta}\right] \tag{A10}$$

we arrive at the following equation:

$$\left\{\left[\mathbf{n}\frac{\partial}{\partial\mathbf{R}} + \frac{1}{l}\right]\delta_{\alpha\gamma} + i(\mathbf{nh})(\hat{\sigma}_z)_{\alpha\gamma}\right\}\Gamma^{(c)}_{\gamma\beta}(\mathbf{R},\mathbf{n}|\mathbf{R}',\mathbf{n}') = \int d\mathbf{n}'' d_{\alpha\gamma}(\mathbf{n},\mathbf{n}'')\Gamma^{(c)}_{\gamma\beta}(\mathbf{R},\mathbf{n}''|\mathbf{R}',\mathbf{n}') + \delta_{\alpha\beta}\delta(\mathbf{R}-\mathbf{R}')\delta(\mathbf{n}-\mathbf{n}'), \tag{A11}$$

where $\hat{\sigma}_z$ entering into Eqs. (A10) and (A11) is the Pauli matrix.

Further we perform the Fourier transform with respect to variable $\mathbf{R}_\parallel - \mathbf{R}'_\parallel$ and expand $\Gamma^{(c)}_{\alpha\beta}$ matrix in spherical harmonics (see, e.g., Refs. [3,47]), keeping only the first two terms,

$$\Gamma^{(c)}_{\alpha\beta}(z,z',\mathbf{q}|\mathbf{n},\mathbf{n}') = \frac{1}{4\pi}[\Gamma^{(c)}_{\alpha\beta}(z,z'|\mathbf{q}) + 3(\mathbf{n}-\mathbf{n}')\mathbf{J}^{(c)}_{\alpha\beta}(z,z'|\mathbf{q})], \tag{A12}$$

where $\Gamma^{(c)}_{\alpha\beta}(z,z'|\mathbf{q})$ is the density propagator (integral over directions) and $\mathbf{J}^{(c)}_{\alpha\beta}(z,z'|\mathbf{q})$ is the corresponding current density. Substituting (A12) into (A11), we obtain the following system of diffusion equations for $\Gamma^{(c)}_{\alpha\beta}(z,z'|\mathbf{q})$:

$$\begin{aligned} &\begin{pmatrix} \left[\left(i\frac{\partial}{\partial z}+h_z\right)^2 + (\mathbf{q}-\mathbf{h}_\parallel)^2\right] + \frac{3}{2}\, n_0^2\sigma_{tr}\sigma_{\rm dep}(1-\chi) & -\frac{3}{2}\, n_0^2\sigma_{tr}\sigma_{\rm dep}(1-\chi) - \chi\left(-\frac{\partial^2}{\partial z^2}+q^2-h^2\right) \\ -\frac{3}{2}\, n_0^2\sigma_{tr}\sigma_{\rm dep}(1-\chi) - \chi\left(-\frac{\partial^2}{\partial z^2}+q^2-h^2\right) & \left[\left(i\frac{\partial}{\partial z}-h_z\right)^2 + (\mathbf{q}+\mathbf{h}_\parallel)^2\right] + \frac{3}{2}\, n_0^2\sigma_{tr}\sigma_{\rm dep}(1-\chi) \end{pmatrix} \\ &\quad\times\begin{pmatrix} \Gamma^{(c)}_{++}(z,z'|\mathbf{q}) & \Gamma^{(c)}_{+-}(z,z'|\mathbf{q}) \\ \Gamma^{(c)}_{-+}(z,z'|\mathbf{q}) & \Gamma^{(c)}_{--}(z,z'|\mathbf{q}) \end{pmatrix} = 3n_0\sigma_{tr}(1-\chi)\begin{pmatrix} 1 & 0 \\ 0 & 1 \end{pmatrix}\delta(z-z'), \end{aligned} \tag{A13}$$

where $\mathbf{h}_\parallel$ and h_z are the components of $\mathbf{h}$ parallel and perpendicular to the sample surface,

$$\sigma_{tr} = \int d\mathbf{n}'\,[1-(\mathbf{nn}')]a_1(\mathbf{nn}') \tag{A14}$$

is the transport scattering cross section,

$$\sigma_{\rm dep} = \int d\mathbf{n}'\,[a_1(\mathbf{nn}') - a_2(\mathbf{nn}')] \tag{A15}$$

is the helicity-flip scattering cross section (see, e.g., Refs. [30,42]),

$$\chi = \frac{\sigma_{tr} - \sigma_{tr}^{(2)} - \sigma_{\rm dep}}{\sigma_{tr} + \sigma_{tr}^{(2)} + \sigma_{\rm dep}}, \tag{A16}$$

$\sigma_{tr}^{(2)} = \int d\mathbf{n}'\,(1 - (\mathbf{n}\mathbf{n}'))a_2(\mathbf{n}\mathbf{n}')$ is the transport scattering cross section [42] appearing in the transport equation for the difference between the intensities of waves with opposite helicity (i.e., for the fourth Stokes parameter [47]).

Under conditions of circular polarization (or helicity) memory [28–32], the difference between the differential scattering cross sections $a_1(\mathbf{n}\mathbf{n}')$ and $a_2(\mathbf{n}\mathbf{n}')$ is small and, as a consequence, $\sigma_{\rm dep} \ll \sigma_{tr}$ and $\sigma_{tr} - \sigma_{tr}^{(2)} \ll \sigma_{tr}$. The parameter χ appearing in Eq. (A13) is also small, $\chi \ll 1$ (e.g., for the Faraday active glass with air bubbles used in experiment [27] the parameter χ calculated with the Mie theory is $\chi = -0.02$). Neglecting the terms proportional to χ in Eq. (A13), we arrive at the diffusion equation (14).

APPENDIX B: CASE OF RAYLEIGH SCATTERING

For the Rayleigh particles Eq. (A8) takes the form

$$\begin{aligned} d_{\pm\pm}(\mathbf{n}\mathbf{n}') &= \frac{3}{32\pi}\, n_0\sigma[1 + (\mathbf{n}\mathbf{n}')]^2, \\ d_{\mp\pm}(\mathbf{n}\mathbf{n}') &= \frac{3}{32\pi}\, n_0\sigma[1 - (\mathbf{n}\mathbf{n}')]^2 \end{aligned} \tag{B1}$$

where $\sigma = \int d\mathbf{n}'\, a_1(\mathbf{n}\mathbf{n}')$ is the scattering cross section. This result can be obtained from Eq. (A9) based on the expressions for the scattering matrix elements a_1 and a_2 (see, e.g., Refs. [47,49]),

$$\begin{aligned} a_1(\mathbf{n}\mathbf{n}') &= \frac{k_0^4 a^6}{18}\,(\epsilon - 1)^2\,[1 + (\mathbf{n}\mathbf{n}')^2], \\ a_2(\mathbf{n}\mathbf{n}') &= \frac{k_0^4 a^6}{9}\,(\epsilon - 1)^2\,(\mathbf{n}\mathbf{n}'). \end{aligned} \tag{B2}$$

In this case $\sigma_{tr} = \sigma_{\rm dep} = \sigma$, $\sigma_{tr}^{(2)} = -\sigma/2$ and $\chi = 1/3$, and Eq. (A13) takes the form

$$\begin{pmatrix} \left[\left(i\frac{\partial}{\partial z} + h_z\right)^2 + (\mathbf{q} - \mathbf{h}_\parallel)^2\right] + n_0^2\sigma^2 & -n_0^2\sigma^2 - \left(-\frac{\partial^2}{\partial z^2} + q^2 - h^2\right)/3 \\ -n_0^2\sigma^2 - \left(-\frac{\partial^2}{\partial z^2} + q^2 - h^2\right)/3 & \left[\left(i\frac{\partial}{\partial z} - h_z\right)^2 + (\mathbf{q} + \mathbf{h}_\parallel)^2\right] + n_0^2\sigma^2 \end{pmatrix} \cdot$$
$$\times \begin{pmatrix} \Gamma_{++}^{(c)}(z, z'|\mathbf{q}) & \Gamma_{+-}^{(c)}(z, z'|\mathbf{q}) \\ \Gamma_{-+}^{(c)}(z, z'|\mathbf{q}) & \Gamma_{--}^{(c)}(z, z'|\mathbf{q}) \end{pmatrix} = 2n_0\sigma \begin{pmatrix} 1 & 0 \\ 0 & 1 \end{pmatrix} \delta(z - z'). \tag{B3}$$

In the absence of the magnetic field, Eq. (B3) can be decoupled into two independent equations for the sum and difference of the elements, $\Gamma_{\pm\pm}^{(c)} + \Gamma_{\mp\pm}^{(c)}$ and $\Gamma_{\pm\pm}^{(c)} - \Gamma_{\mp\pm}^{(c)}$. The sum $\Gamma_{\pm\pm}^{(c)} + \Gamma_{\mp\pm}^{(c)}$ decays over great distances of the order of $1/q$ while the difference $\Gamma_{\pm\pm}^{(c)} - \Gamma_{\mp\pm}^{(c)}$ decays rapidly over distances of the order of the mean-free path. In the diffusion regime the value of $\Gamma_{\pm\pm}^{(c)} - \Gamma_{\mp\pm}^{(c)}$ should be neglected and therefore all elements $\Gamma_{\alpha\beta}^{(c)}$ proves to be equal to each other. They decay over distances of the order of $1/q$ [17].

In the presence of the magnetic field, the qualitative picture remains the same, but the specific expressions for $\Gamma_{\alpha\beta}^{(c)}$ begin to depend on the magnetic field. In particular, in the case of the magnetic field parallel to the sample surface, the values of $\Gamma_{\alpha\beta}^{(c)}$ are determined by the relations

$$\begin{aligned} \Gamma_{\pm\pm}(z, z'|\mathbf{q}) &= \tfrac{1}{2}\, P(z, z'|\mathbf{q})\,(1 \mp 2(\mathbf{q}\mathbf{h})l^2), \\ \Gamma_{\mp\pm}(z, z'|\mathbf{q}) &= \tfrac{1}{2}\, P(z, z'|\mathbf{q}), \end{aligned} \tag{B4}$$

where $l = (n_0\sigma)^{-1}$ is the mean-free path. The function $P(z, z'|\mathbf{q})$ is subject to Eq. (23) with $\gamma = \sqrt{q^2 + 2h^2}$ [17] and it is assumed that q and $h \ll 1/l$.

The CBS angular profile [see Eq. (9)] that corresponds to Eq. (B4) is also expressed in terms of $J_{\rm scal}^{(c)}(\gamma)$. For example, the CBS intensity in the helicity-preserving channel has the form

$$J_{\pm\pm}^{(c)}(\mathbf{q}) = \tfrac{1}{2}\, J_{\rm scal}^{(c)}(\sqrt{q^2 + 2h^2})[1 \mp 2(\mathbf{q}\mathbf{h})l^2]. \tag{B5}$$

The total intensity for coherent backscattering of linearly polarized light is

$$J_{\rm tot}^{(c)}(\mathbf{q}) = J_{\rm scal}^{(c)}(\sqrt{q^2 + 2h^2}). \tag{B6}$$

The results (B5) and (B6) remain valid also for the magnetic field perpendicular to the sample surface (in this case $\mathbf{q}\mathbf{h} = 0$). Equation (B6) coincides with the principal (i.e., diffusion) contribution to the result obtained in Refs. [17,19].

[1] G. Bergmann, Weak localization in thin films, Phys. Rep. **107**, 1 (1984).

[2] C. W. J. Beenakker, Random-matrix theory of quantum transport, Rev. Mod. Phys. **69**, 731 (1997).

[3] E. Akkermans and G. Montambaux, *Mesoscopic physics of electrons and photons* (Cambrige, University Press, Cambridge, 2007).

[4] C. M. Aegerter and G. Maret, Coherent backscattering and Anderson localization of light, Progress in Optics, **52**, 1 (2009).

[5] B. L. Altshuler, D. E. Khmelnitskii, A. I. Larkin, and P. A. Lee, Magnetoresistance and Hall effect in a disordered two-dimensional electron gas, Phys. Rev. B **22**, 5142 (1980).

[6] B. L. Altshuler, A. G. Aronov, D. E. Khmel'nitskii, and A. I. Larkin, *Quantum Theory of Solids* (Mir, Moscow, 1982), p. 130.

[7] O. Sigwarth, G. Labeyrie, T. Jonckheere, D. Delande, R. Kaiser, and C. Miniatura, Magnetic Field Enhanced Coherence Length in Cold Atomic Gases, Phys. Rev. Lett. **93**, 143906 (2004).

[8] R. V. Mehta, R. Patel, and R. V. Upadhyay, Direct observation of magnetically induced attenuation and enhancement of coherent backscattering of light, Phys. Rev. B **74**, 195127 (2006).

[9] K. Y. Bliokh, S. A. Gredeskul, P. Rajan, I. V. Shadrivov, and Y. S. Kivshar, Nonreciprocal Anderson localization in magneto-optical random structures, Phys. Rev. B **85**, 014205 (2012).

[10] A. Christofi and N. Stefanou, Nonreciprocal optical response of helical periodic structures of plasma spheres in a static magnetic field, Phys. Rev. B **87**, 115125 (2013).

[11] Y. Bromberg, B. Redding, S. M. Popoff, and H. Cao, Control of coherent backscattering by breaking optical reciprocity, Phys. Rev. A **93**, 023826 (2016).

[12] L. Schertel, G. J. Aubry, C. M. Aegerter, and G. Maret, Coherent multiple light scattering in Faraday active materials, Eur. Phys. J. Special Topics **226**, 1409 (2017).

[13] L. Schertel, O. Irtenkauf, C. M. Aegerter, G. Maret, and G. J. Aubry, Magnetic-field effects on one-dimensional Anderson localization of light, Phys. Rev. A **100**, 043818 (2019).

[14] E. Akkermans, P. E. Wolf, R. Maynard, and G. Maret, Theoretical study of the coherent backscattering of light by disordered media, J. Phys. (Paris) **49**, 77 (1988).

[15] M. B. van der Mark, M. P. van Albada, and A. Lagendijk, Light scattering in strongly scattering media: Multiple scattering and weak localization, Phys. Rev. B **37**, 3575 (1988).

[16] M. C. W. van Rossum and T. M. Nieuwenhuizen, Multiple scattering of classical waves: microscopy, mesoscopy, and diffusion, Rev. Mod. Phys. **71**, 313 (1999).

[17] A. A. Golubentsev, Suppression of interference effects in multiple scattering of light, Sov. Phys. JETP **59**, 26 (1984).

[18] A. A. Golubentsev, Interference correction to the albedo of a strongly gyrotropic medium with random inhomogeneities, Radiophys. Quantum Electron. **27**, 506 (1984).

[19] F. C. MacKintosh and S. John, Coherent backscattering of light in the presence of time-reversal-noninvariant and parity-nonconserving media, Phys. Rev. B **37**, 1884 (1988).

[20] A. S. Martinez and R. Maynard, Faraday effect and multiple scattering of light, Phys. Rev. B **50**, 3714 (1994).

[21] R. Lenke, and G. Maret, Affecting weak light localization by strong magnetic fields, Phys. Scr. **T49B**, 605 (1993).

[22] R. Lenke and G. Maret, Magnetic field effects on coherent backscattering of light, Eur. Phys. J. B **17**, 171 (2000).

[23] F. A. Erbacher, R. Lenke, and G. Maret, Multiple light scattering in magneto-optically active media, Europhys. Lett. **21**, 551 (1993).

[24] B. A. van Tiggelen, R. Maynard, and T. M. Nieuwenhuizen, Theory for multiple light scattering from Rayleigh scatterers in magnetic fields, Phys. Rev. E **53**, 2881 (1996).

[25] D. Lacoste and B. A. van Tiggelen, Coherent backscattering of light in a magnetic field, Phys. Rev. E **61**, 4556 (2000).

[26] F. A. Pinheiro, A. S. Martinez, and L. C. Sampaio, New Effects in Light Scattering in Disordered Media and Coherent Backscattering Cone: Systems of Magnetic Particles, Phys. Rev. Lett. **84**, 1435 (2000).

[27] R. Lenke, R. Lehner, and G. Maret, Magnetic-field effects on coherent backscattering of light in case of Mie spheres, Europhys. Lett. **52**, 620 (2000).

[28] F. C. MacKintosh, J. X. Zhu, D. J. Pine, and D. A. Weitz, Polarization memory of multiply scattered light, Phys. Rev. B **40**, 9342 (1989).

[29] D. Bicout, C. Brosseau, A. S. Martinez, and J. M. Schmitt, Depolarization of multiply scattered waves by spherical diffusers: Influence of the size parameter, Phys. Rev. E **49**, 1767 (1994).

[30] E. E. Gorodnichev, A. I. Kuzovlev, and D. B. Rogozkin, Diffusion of circularly polarized light in a disordered medium with large-scale inhomogeneities, JETP Lett. **68**, 22 (1998).

[31] M. K. Schmidt, J. Aizpurua, X. Zambrana-Puyalto, X. Vidal, G. Molina-Terriza, and J. J. Saenz, Isotropically Polarized Speckle Patterns, Phys. Rev. Lett. **114**, 113902 (2015).

[32] E. E. Gorodnichev, A. I. Kuzovlev, and D. B. Rogozkin, Anomalous depolarizing properties of a disordered ensemble of resonant Mie particles, JETP Lett. **104**, 157 (2016).

[33] A. K. Zvezdin and V. A. Kotov, *Modern magnetooptics and magnetooptical materials* (Institute of Physics Publishing, London, 1997), p. 404.

[34] D. Vojna, O. Slezak, A. Lucianetti, and T. Mocek, Verdet constant of magneto-active materials developed for high-power Faraday devices, Appl. Sci. **9**, 3160 (2019).

[35] E. E. Gorodnichev and D. B. Rogozkin, Quantum interference in the backscattering of charged particles from a disordered medium in a magnetic field, Sov. Phys. JETP **73**, 557 (1991); Quantum interference phenomena in electron backscattering by a random medium in a magnetic field, Physica B **179**, 312 (1992).

[36] M. J. Stephen and G. Cwilich, Rayleigh scattering and weak localization: Effects of polarization, Phys. Rev. B **34**, 7564 (1986).

[37] K. J. Peters, Coherent-backscatter effect: A vector formulation accounting for polarization and absorption effects and small or large scatterers, Phys. Rev. B **46**, 801 (1992).

[38] All propagators related to the interference contribution are assumed to contain two or more scattering events (see, e.g., Ref. [3]).

[39] E. E. Gorodnichev, A. I. Kuzovlev, and D. B. Rogozkin, Coherent backscattering of polarized light from a turbid medium, JETP **106**, 731 (2008).

[40] Depolarization of linearly polarized light is governed by the modes decaying over distances of the order of the transport mean-free path l_{tr} [41,42]. The calculation of these modes is beyond the diffusion theory (see, e.g., Refs. [41,42]).

[41] M. I. Mishchenko, L. D. Travis, and A. A. Lacis, *Multiple Scattering of Light by Particles* (Cambridge University Press, Cambridge, 2006).

[42] E. E. Gorodnichev, A. I. Kuzovlev, and D. B. Rogozkin, Depolarization coefficients of light in multiply scattering media, Phys. Rev. E **90**, 043205 (2014).

[43] M. I. Mishchenko, Polarization effects in weak localization of lifgt: Calculation of the copolarized and depolarized backscattering enhancement factors, Phys. Rev. B **44**, 12597 (1991).

[44] R. J. Potton, Reciprocity in optics, Rep. Prog. Phys. **67**, 717 (2004).

[45] K. Pandey, C. C. Kwong, M. S. Pramod, and D. Wilkowski, Linear and nonlinear magneto-optical rotation on the narrow strontium intercombination line, Phys. Rev. A **93**, 053428 (2016).

[46] H. Goldstein, *Classical Mechanics*, 3rd ed. (Addison-Wesley, Boston, 2002).

[47] H. C. van de Hulst, *Multiple Light Scattering: Tables, Formulas, and Applications* (Academic Press, New York, 1980).

[48] M. Kerker, D-S. Wang, and C. L. Giles, Electromagnetic scattering by magnetic spheres, JOSA **73**, 765 (1983).

[49] R. G. Newton, *Scattering Theory of Waves and Particles*, 2nd ed. (Springer, New York, 1982).

[50] V. B. Berestetskii, E. M. Lifshitz, and L. P. Pitaevskii, *Quantum Electrodynamics: Vol. 4, Course of Theoretical Physics* (Pergamon Press, Oxford, 1982).

[51] K. Vynck, R. Pierrat, and R. Carminati, Polarization and spatial coherence of electromagnetic waves in uncorrelated disordered media, Phys. Rev. A **89**, 013842 (2014); Multiple scattering of polarized light in disordered media exhibiting short-range structural correlations, **94**, 033851 (2016).